Size Assessment of Power Cable Shield Corrosion Defects Using Double-Frequency Time–Frequency-Domain Reflectometry

Size Assessment of Power Cable Shield Corrosion Defects Using Double-Frequency Time-Frequency Domain Reflectometry

Kun Zhao, *Student member, IEEE*, Stefano Grivet-Talocia, *Fellow, IEEE*, Paolo Manfredi, *Senior Member, IEEE*, Yuan Yan and Hongjie Li

***Abstract*—Cable shield corrosion defects are a common threat to power cables, requiring precise detection and sizing for effective management. Such defect detection and location methods are widely researched. However, essentially none of them can accurately assess the length of shield corrosion defects. To solve this issue, we develop a model to represent the impact of shield corrosion. Building upon this model, we propose a double-frequency time-frequency domain reflectometry (TFDR) method. The innovation of double-frequency TFDR lies in conducting two successive measurements, with the center frequency of the second signal being twice that of the first. The length of the shield corrosion defects is determined by analyzing the measured signals using the spectrum ratio. The proposed method is validated through simulations on a 10-kV system and experiments with a SYV50-type cable. The results show that estimation errors for the defects' equivalent inductance and length are below 2% and 0.3%, respectively. Hence, double-frequency TFDR emerges as a powerful tool for assessing cable shield corrosion.**

***Index Terms*—Cable defects, defect assessment, defect detection, shield corrosion, time-frequency domain reflectometry.**

I. Introduction

WITHIN the framework of national infrastructure development, the electric power system plays a crucial role in ensuring the stability and safety of countries. In contemporary electric power systems, cables serve as the primary means of power transmission, particularly within urban distribution grids. Consequently, within the national emergency management framework, maintaining cable safety is a critical responsibility for electric power companies, as it is integral to ensuring the reliability and security of the power supply system.

Distribution power cables, located underground, are vulnerable to damage, moisture [1], and high temperatures [2]–[4]. These adversities can precipitate many cable defects and shield corrosion is one of the typical defects. Corrosion defects have three main associated risks: 1) Inducing insulation faults [5]; 2) Interfering with the accurate location of faults and partial discharges [6]; 3) Affecting power quality [7]. Therefore, accurately locating and evaluating cable shield corrosion defects are crucial for maintaining the stable operation of the power system.

To detect shield corrosion defects, the IEEE guide for the corrosion of metallic cable shields [6] provides four methods: the visual inspection method, the concentric neutral resistance measurement method, the surface voltage measurement technique, and the reflectometry method. Among the methods mentioned above, the reflectometry-based techniques demonstrate superior performance in detecting and evaluating copper shield corrosion defects due to their rapid detection and localization capabilities [4], [8], [9].To detect and assess the shield corrosion defects using reflectometry-based techniques, it is necessary to build a model of the shield corrosion defects and study the relationship between the reflected signals and these defects. Numerical methods like the finite element method (FEM), the method of moments, and the finite-difference time-domain method [10], [11] are suitable and not limited by the shape of the defects. However, they are unable to describe the relationship between the size of the corrosion and the reflection characteristics in an analytical manner. In [12], [13], the current in the shield corrosion defect was analyzed and considered to flow in a spiral pattern. Based on this result, an equivalent inductance was introduced to describe the corrosion defects, but no method was provided to calculate the inductance. In [14], an equivalent inductor model of shield corrosion was proposed; however, it was neither explained nor validated. Moreover, a formula to calculate the equivalent inductance was derived in [15], but its impact on the propagation characteristic of the entire cable was not analyzed. Therefore, it is essential to establish an equivalent circuit for shield corrosion defects and analyze the effect of these defects on the propagation characteristics of the entire cable.

Time-domain reflectometry (TDR) and frequency-domain reflectometry (FDR) are the two most common types of reflectometry-based methods used for detecting power cable defects [16], [17]. TDR was the first to be implemented and is characterized by limited sensitivity, which only allows the detection and rough evaluation of significant corrosion defects [6], [10]. FDR provides higher sensitivity but suffers from complex localization methods and poorer spatial resolution, complicating the accurate evaluation of defect sizes. Despite

This work was supported in part by the China Scholarship Council. (Corresponding author: Kun Zhao).

Kun Zhao and Yuan Yan are with the State Key Laboratory of Insulation and Power Equipment, School of the Electrical Engineering, Xi'an Jiaotong University, Xi'an 710049, China, and also with the Department of Electronics and Telecommunications, Politecnico di Torino, Turin 10129 , Italy (e-mail: zhaokun@stu.xjtu.edu.cn; y220928y@stu.xjtu.edu.cn).

Stefano Grivet-Talocia and Paolo Manfredi are with the Department of Electronics and Telecommunications, Politecnico di Torino, Turin 10129, Italy (e-mail: stefano.grivet@polito.it; paolo.manfredi@polito.it).

Hongjie Li is with the State Key Laboratory of Insulation and Power Equipment, School of the Electrical Engineering, Xi'an Jiaotong University, Xi'an 710049, China (e-mail: hjli@mail.xjtu.edu.cn)

Manuscript received April 19, 2021; revised August 16, 2021.

these technological advancements, time-frequency domain reflectometry (TFDR) has emerged as a more effective method due to its enhanced sensitivity and spatial resolution, which are crucial for accurately detecting and locating corrosion-related defects [18], [19]. In [20], [21], an improved location algorithm based on the cross-correlation method was developed, significantly improving the location accuracy of TFDR. Furthermore, [22] proposed a classification method using cross-correlation to distinguish different types of faults. [23] analyzed how the severity of defects affects the strength of reflected signals using neural networks. In [18], [24], the relationship between defect sizes and the correlation coefficient of the injected and reflected signals was explored, and the influence of defects on the reflected signals was analyzed only qualitatively. In summary, despite these advancements, a robust and precise method for detecting and evaluating the size of cable shield corrosion defects is still lacking.

To solve the above problems, we propose an approach for detecting cable shield corrosion defects and determining their size using double-frequency TFDR. Our method involves conducting two consecutive measurements with a TFDR signal, where the center frequency is doubled in the second measurement. The size of the shield corrosion defects is then accurately determined based on the spectrum ratio between the injected and reflected signals from the two measurements. The key contributions are as follows:

1) To characterize cable shield corrosion, an equivalent circuit model of shield corrosion defects is established, and the parameters in the model are derived.
2) To examine the impact of shield corrosion defects on reflected signals, the defect transfer function is derived from the established shield corrosion models. Following this derivation, the localization results from the time-frequency cross-correlation (TFCC) are analyzed, revealing that TFCC identifies the midpoint of the defects rather than their starting points.
3) To assess the size of shield corrosion defects, a double-frequency TFDR approach is introduced for detecting cable shield corrosion. This method accurately calculates the defect length and the characteristic impedance from measurements.

The remainder of this article is structured as follows. Section II outlines the theoretical foundations of TFDR and TFCC, followed by the establishment of a cable shield corrosion model. Utilizing these models, the transfer function for shield corrosion and the formulation for defect location results via TFCC methods are derived. Subsequently, a method for assessing the shield corrosion size using double-frequency TFDR is introduced, accompanied by a flowchart detailing the double-frequency TFDR procedure. In Section III, the simulation of a 10-kV cable validates the proposed cable shield corrosion models and the accuracy of size assessment of double-frequency TFDR, also showcasing the double-frequency TFDR process in full. Section IV describes an experimental setup, with a statistical analysis and discussion of the experimental errors. The article concludes with Section V, which summarizes the findings and the implications of the study.

II. Theoretical background

A. Basic Theory of Cable Defect Detection Using TFDR

The method of TFDR employs a Gaussian-enveloped linear frequency-modulated signal to detect cable defects. The injection signal is expressed as [25]

$$s\left(t\right)=A\cdot e^{\frac{-\alpha\left(t-t_0\right)^2}{2}+j\frac{\beta\left(t-t_0\right)^2}{2}+j\omega_0\left(t-t_0\right)}, \tag{1}$$

where the parameter α defines the duration of $s\left(t\right)$, while β controls the slope of its instantaneous frequency. The variable t_0 denotes the time center of $s\left(t\right)$, and ω_0 represents its center frequency. Additionally, A is associated with the amplitude of $s\left(t\right)$.

As the signal $s\left(t\right)$ travels through a cable with defects, it is reflected, creating a reflected signal $r\left(t\right)$ due to the defects. The location of these defects can be pinpointed using the TFCC method [26]. When using TFCC to analyze the signals, both the injected and reflected signals must be transformed from the time domain to the time-frequency domain to obtain their time-frequency distributions. For time-frequency analysis of linear frequency-modulated signals, the Wigner-Ville distribution (WVD) method provides the best time-frequency resolution. Thus, the WVD method is utilized in TFCC for acquiring the time-frequency distribution. The WVD distribution $W_s\left(t,\omega\right)$ of the injected signal $s\left(t\right)$ is defined as [27]

$$\begin{aligned}W_s\left(t,\omega\right)&=\int_{-\infty}^{+\infty}s\left(t+\frac{\tau}{2}\right)s^*\left(t-\frac{\tau}{2}\right)e^{-j\tau\omega}d\tau\\&=2A^2\sqrt{\frac{\pi}{\alpha}}e^{-\alpha\left(t-t_0\right)^2-\frac{1}{\alpha}\left(\omega-\beta\left(t-t_0\right)-\omega_0\right)}.\end{aligned} \tag{2}$$

The expression of the TFCC between the injected signal $s\left(t\right)$ and the reflected signal $r\left(t\right)$ reads (3)

$$C_{sr}\left(t\right)=\frac{2\pi}{E_sE_r\left(t\right)}\times\int_{t'=t-T_s}^{t'=t+T_s}\int_{-\infty}^{+\infty}W_r\left(t',\omega\right)W_s\left(t'-t,\omega\right)d\omega dt', \tag{3a}$$

$$E_s=\iint W_s\left(t,\omega\right)dtd\omega, \tag{3b}$$

$$E_r\left(t\right)=\int_{t'=t-T_s}^{t'=t+T_s}\int_{-\infty}^{+\infty}W_r\left(t',\omega\right)d\omega dt'. \tag{3c}$$

The terms $W_r(t,\omega)$ represent the WVD of the reflected signal $r(t)$, which can be derived in the same way as $W_s(t,\omega)$. The variables E_s and $E_r(t)$ are utilized to normalize $C_{sr}(t)$, ensuring that $C_{sr}(t)$ is bounded between 0 and 1. T_s controls the integral length, which $T_s=3\sigma_t$ and [19]

$$\sigma_t^2=\int_{-\infty}^{\infty}\left(t-t_0\right)^2\mid s\left(t\right)\mid^2dt. \tag{4}$$

If the cable exhibits defects, the $C_{sr}(t)$ curve will feature peak points corresponding to the arrival times of signals reflected by the defects. Subsequently, the location of the defects can be determined using the wave propagation velocity.

B. Modeling of Cable Shield Corrosion Defects

In this section, we introduce a model of shield corrosion defects. Before proceeding with the defect modeling, analyzing the distributed-parameter model for healthy cables is crucial. This work focuses on a typical power cable structured with a circular core conductor, multiple insulating layers, and an outer shield, which is shown as Fig. 1 [28].

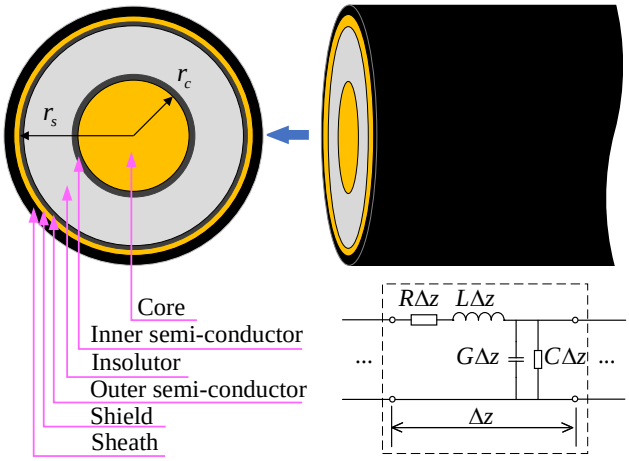

Fig. 1. The structure of the single-core power cable.

In Fig. 1, R, L, G, and C represent the cable's per-unit-length resistance, inductance, conductance, and capacitance, respectively. r_c and r_s are the radius of the core and shield, respectively. The cable geometry and electrical properties determine these parameters. The expressions for these parameters are provided as follows [29]

$$R(\omega) \approx \frac{1}{2\sqrt{2}\pi r_c}\sqrt{\omega\mu_0\sigma_c} + \frac{1}{2\sqrt{2}\pi r_s}\sqrt{\omega\mu_0\sigma_s}, \tag{5}$$

$$L(\omega) = \frac{1}{4\pi r_c}\sqrt{\frac{2\mu_0\sigma_c}{\omega}} + \frac{1}{4\pi r_s}\sqrt{\frac{2\mu_0\sigma_s}{\omega}} + \frac{\mu_0}{2\pi}\ln\frac{r_s}{r_c}, \tag{6}$$

$$G(\omega) = \Re\left(\frac{1}{\sum_{k=1}^{N}\frac{1}{Y_k(\omega)}}\right), \tag{7}$$

$$C(\omega) = \Im\left(\frac{1}{\omega\sum_{k=1}^{N}\frac{1}{Y_k(\omega)}}\right), \tag{8}$$

where N indicates the number of insulating layers, μ is the vacuum permeability, whereas σ_c and σ_s are the resistivities of the cable core and shield, respectively. Moreover, $Y_k(\omega)$ is the admittance of the k-th insulating layer, defined as [30]

$$Y_k(\omega) = j\omega\epsilon_k(\omega)\frac{2\pi}{\ln\left(\frac{r_{k+1}}{r_k}\right)}, \tag{9}$$

where ϵ_k is the complex permittivity of the k-th insulating layer, whereas r_k and r_{k+1} are the radii of the k-th and $(k+1)$-th insulating layers, respectively.

1) Model of shield corrosion: Given the copper tape-wrapped structure of the cable shield, the corrosion results in a patina forming on the copper tape surface and between two adjacent layers of shielding tape. An illustration of a cable experiencing shield corrosion is provided in Fig. 2.

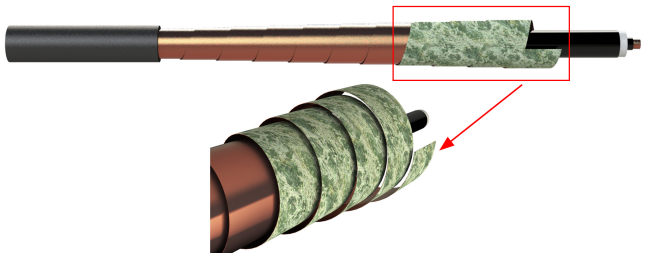

Fig. 2. Illustration of cable with shield corrosion.

Patina, characterized by its low conductivity, serves to insulate the adjacent layers of copper tape from each other [31]. As the current in the cable shield follows a spiral path, an additional equivalent inductance is induced by this spiral current [15]. The distributed-parameter model of the cable with shield corrosion defects is modified as shown in Fig. 3.

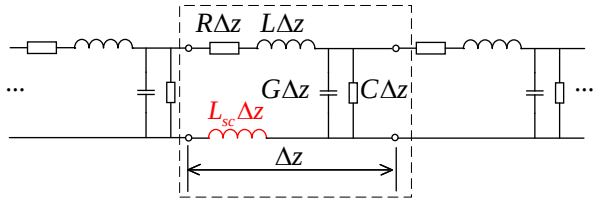

Fig. 3. Distributed-parameter model of cable with shield corrosion.

The corroded shield can be likened to a solenoid coil; therefore, we can use the method for calculating the inductance of a solenoid coil to determine the additional equivalent inductance. To calculate the equivalent inductance, the structure of the spiral shield must be defined. The geometric parameters of the spiral shield are depicted in Fig. 4, where M_s and M_h represent the width and pitch distance of the copper tape, respectively, and d_s is the diameter of the cable insulator. The equations for calculating the inductance of a solenoid coil are described in [32]

$$L_{sc} = N_s\frac{\Phi_s}{I_s}, \tag{10a}$$

$$\Phi_s = B_s S_s. \tag{10b}$$

Where Φ_s is the magnetic flux in the solenoid coil, and I_s is the current. N_s represents the number of turns of the copper shield on a 1-meter-long cable, B_s is the magnetic flux density,

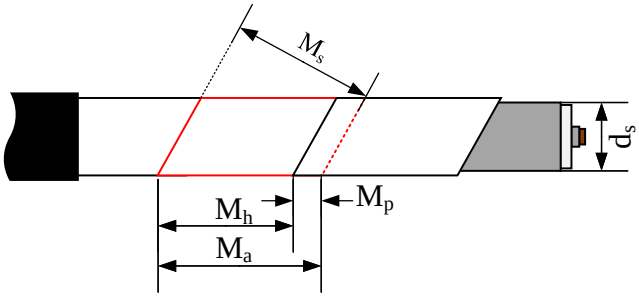

Fig. 4. Geometric parameters of the equivalent solenoid coil.

and S_s is the cross-sectional area of the solenoid coil. These quantities are expressed as follows

$$N_s = \frac{1}{M_h}, \tag{11}$$

$$B_s = \mu_0 \frac{1}{M_h}, \tag{12}$$

$$S_s = \pi \left(\frac{d_s}{2}\right)^2. \tag{13}$$

Usually, M_h is unknown; however, the overlap ratio $\rho = M_p/M_a$ of the wrapped shield is provided in the cable handbook [6]. Therefore, M_h can be derived using ρ as follows

$$M_h = \frac{\pi d_s (1-\rho) M_s}{\sqrt{(\pi d_s)^2 - (1-\rho)^2 M_s^2}}. \tag{14}$$

By substituting (11), (12), (13), and (14) into (10), the additional equivalent inductance caused by the corroded shield can be derived as follows

$$L_{sc} = \frac{\mu_0}{4\pi} \frac{(\pi d_s)^2 - (1-\rho)^2 M_s^2}{(1-\rho)^2 M_s^2}. \tag{15}$$

The per-unit-length inductance of a cable with shield corrosion is expressed as

$$L_s(\omega) \approx \frac{1}{4\pi r_c}\sqrt{\frac{2\mu_0\sigma_c}{\omega}} + \frac{1}{4\pi r_s}\sqrt{\frac{2\mu_0\sigma_s}{\omega}} + \frac{\mu_0}{2\pi}\ln\frac{r_s}{r_c} + \frac{\mu_0}{4\pi}\frac{(\pi d_s)^2 - (1-\rho)^2 M_s^2}{(1-\rho)^2 M_s^2}. \tag{16}$$

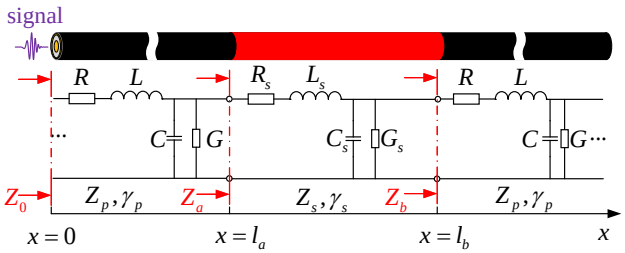

Fig. 5. Distributed-parameter model of a long cable with shield corrosion defects. Z_0, Z_a, and Z_b represent the input impedance of the cable at $x = 0$, $x = l_a$, and $x = l_b$, respectively. Z_p and γ_p denote the characteristic impedance and propagation constant of a healthy cable. Z_s and $\gamma_s = \alpha_s + j\beta_s$ refer to the characteristic impedance and propagation constant of a cable affected by shield corrosion, respectively, where α_s is the attenuation constant and β_s is the phase constant.

2) Model of reflection from shield corrosion defects in a cable: The distributed-parameter model of a long cable with shield corrosion is shown in Fig. 5. According to the transmission line theory and assuming a cable of infinite length, the input impedance is expressed as

$$Z_a = Z_s \frac{1 + \Gamma_b e^{-2\gamma_s l_c}}{1 - \Gamma_b e^{-2\gamma_s l_c}}, \tag{17}$$

where

$$\Gamma_b = \frac{Z_p - Z_s}{Z_p + Z_s} \tag{18}$$

and

$$\Gamma_a = \frac{Z_a - Z_p}{Z_a + Z_p} = \frac{-\Gamma_b + \Gamma_b e^{-2\gamma_s l_c}}{1 - {\Gamma_b}^2 e^{-2\gamma_s l_c}} \tag{19}$$

are the reflection coefficient at $x = l_b$ and $x = l_a$, whereas $l_c = l_b - l_a$ is the length of shield corrosion.

The characteristic impedance Z_s of a cable with shield corrosion defects is not significantly different from that of a perfect cable, thus, Γ_b satisfies the condition $|\Gamma_b| < 1$, and as a result, ${\Gamma_b}^2 \ll 1$. Furthermore, $|e^{-2\gamma_s l_c}| < 1$, which implies that ${\Gamma_b}^2 e^{-2\gamma_s l_c} \approx 0$. Consequently, by ignoring the signal attenuation, the expression of Γ_a can be approximated as

$$\Gamma_a \approx -\Gamma_b + \Gamma_b e^{-2j\beta_s l_c} = -2\Gamma_b \sin(\beta_s l_c) e^{j\left(\frac{\pi}{2} - \beta_s l_c\right)}. \tag{20}$$

C. Detection and Size Assessment of Shield Corrosion

1) Location of shield corrosion defects using TFCC: To detect and locate defects in a cable with shield corrosion using TFDR, it is crucial to examine the impact on the reflected signals of a defect at $x = l_a$. Once the signal is injected into the cable at the start terminal ($x = 0$), as illustrated in Fig. 5, the time-domain reflected signal $r(t)$ corresponding to the defects at the start terminal can be derived as

$$r(t) = \mathcal{F}^{-1}\{S(\omega) \cdot H_p(\omega, l_a) \cdot \Gamma_a(\omega)\}, \tag{21}$$

where $\mathcal{F}^{-1}$ represents the inverse Fourier transform, $S(\omega)$ is the spectrum of $s(t)$ in (1), and $H_p(\omega, l_a)$ denotes the transfer function of a l_a-long healthy cable, defined as $H_p(\omega, l_a) = e^{-j(K_p - jA_p)\omega 2l_a}$ [20].

Assuming a linear frequency dependence for the phase constant, i.e., $\beta_s = K_s\omega$ [25], Γ_a is expressed as

$$\Gamma_a = -2\Gamma_b \sin(K_s l_c \omega) e^{j\left(\frac{\pi}{2} - K_s l_c \omega\right)}. \tag{22}$$

The reflected signal $r(t)$ is thus derived to be

$$r(t) = -\Gamma_b A e^{\frac{\omega'^2 - \omega_0^2}{2(\alpha - j\beta)}} \times \left(e^{-\frac{\alpha}{2}(t-t')^2 + \frac{j\beta}{2}(t-t')^2 + j\omega'(t-t')} - e^{-\frac{\alpha}{2}(t-t'')^2 + \frac{j\beta}{2}(t-t'')^2 + j\omega'(t-t'')}\right), \tag{23}$$

where

$$\omega' = \omega_0 - \frac{\alpha^2 + \beta^2}{\alpha} A_p 2l_a, \tag{24a}$$

$$t' = t_0 + 2K_p l_a - \frac{\beta}{\alpha} A_p 2l_a, \tag{24b}$$

$$t'' = t_0 + 2K_p l_a + 2K_s l_c - \frac{\beta}{\alpha} A_p 2l_a. \tag{24c}$$

According to (2) and (3), the defects can be located based on $C_{sr}(t)$. The expression of $C_{sr}(t)$ reads

$$C_{st}(t) = \frac{\frac{1}{2}c_1(t) - A_1 c_1(t - K_s l_c) + \frac{1}{2}c_1(t - 2K_s l_c)}{1 - A_2}, \tag{25}$$

with

$$c_1(t) = e^{-\frac{\alpha^2+\beta^2}{2\alpha}(2A_p l_a)^2} e^{-\frac{\alpha^2+\beta^2}{2\alpha}(t-2K_p l_a)^2}, \tag{26a}$$

$$A_1 = e^{-\frac{\alpha^2+\beta^2}{2\alpha}\left((2A_p l_a)^2+(K_s l_c)^2\right)} \times \cos\left(2K_s l_c\left(\omega_0 - \frac{\alpha^2+\beta^2}{\alpha} A_p l_a\right)\right), \tag{26b}$$

$$A_2 = e^{-\frac{\alpha^2+\beta^2}{\alpha}(K_s l_c)^2} \times \cos\left(2K_s l_c\left(\omega_0 - \frac{\alpha^2+\beta^2}{\alpha} 2A_p l_a\right)\right). \tag{26c}$$

The arrival time of the reflected signal due to defects is indicated by the peak points on $C_{sr}(t)$. The time t_p associated with these peak points is given by

$$t_p = 2K_p l_a + K_s l_c. \tag{27}$$

In (27), it is observed that the location result pinpoints the midpoint of shield corrosion defects rather than their onset. Following the defect localization, the focus shifts towards evaluating the severity and determining the size of these defects. Consequently, methods for assessing the size of cable shield corrosion are explored.

2) Size assessment of shield corrosion defects based on double-frequency TFDR: To evaluate the severity and size of the shield corrosion, the spectrum ratio of the reference signal and the reflected signal are calculated [33]. The spectrum function of the injected signal $S(\omega)$ is derived as

$$S(\omega) = A\sqrt{\frac{2\pi}{\alpha - j\beta}} e^{-\frac{(\omega-\omega_0)^2}{2(\alpha-j\beta)} - j\omega t_0}. \tag{28}$$

The spectrum function $R(\omega)$ of the reflected signal $r(t + 2K_p l_a + K_s l_c)$ that can be extracted from $r(t)$ based on the location results of $C_{sr}(t)$ is shown as follows

$$R(\omega) = A\sqrt{\frac{2\pi}{\alpha - j\beta}} e^{-\frac{(\omega-\omega_0)^2}{2(\alpha-j\beta)} - j\omega t_0 - 2A_p l_a \omega} \times \left(-2\Gamma_b \sin(K_s l_c \omega) e^{j\frac{\pi}{2}}\right). \tag{29}$$

The spectrum ratio between reflected and injected signals is defined as

$$P_{sr}(\omega) = \frac{R(\omega)}{S(\omega)} = -2\Gamma_b \sin(K_s l_c \omega) e^{-2A_p l_a \omega} e^{j\frac{\pi}{2}}. \tag{30}$$

In (30), the term $\Gamma_b \sin(K_s l_c \omega)$ is determined solely by the intrinsic parameters of the defect, i.e., Γ_b, K_s, and l_c. Therefore, this term is defined as the corrosion ratio C_r, which quantifies the degree of shield corrosion:

$$C_r = \Gamma_b \sin(K_s l_c \omega). \tag{31}$$

Upon analyzing (31), conducting two consecutive measurements on the cable, in which the center frequency of the signal is doubled, enables the measurement of the defect length l_c. Consequently, we propose a double-frequency TFDR method for detecting cable shield corrosion defects and assessing their sizes. In this double-frequency TFDR approach, the equations for calculating l_c of defects are presented as

$$\cos(K_s l_c \omega) = \frac{\Gamma_b \sin(K_s l_c 2\omega)}{2\Gamma_b \sin(K_s l_c \omega)} = \frac{C_{r2}}{2C_{r1}}, \tag{32a}$$

$$l_c = \frac{1}{K_s \omega} \arccos\left(\frac{C_{r2}}{2C_{r1}}\right), \tag{32b}$$

where C_{r1} represents the corrosion ratio C_r measured during the first measurement, and C_{r2} is the measured result of C_r during the second measurement, which is conducted at twice the center frequency of the first measurement.

C_r can be measured using TFDR as outlined in (30), leading to

$$C_r = \frac{|P_{sr}|}{2e^{-2A_p l_a \omega}}. \tag{33}$$

In this context, it becomes essential to compute $e^{-2A_p l_a \omega}$. $A_p\omega = \alpha_p$ represents the attenuation constant of the healthy cable, which can be determined using TFDR on a healthy cable as follows

$$\alpha_p = -\frac{1}{2l_x} \cdot \frac{1}{2} \ln \frac{\int W_r(t,\omega)\, dt}{\int W_s(t,\omega)\, dt}. \tag{34}$$

Where l_x is the length of the healthy cable used for measuring α_p measurement. $W_r(t,\omega)$ is the Wigner-Ville distribution of the reflected signal from the open-circuit end of the healthy cable, and $W_s(t,\omega)$ is the Wigner-Ville distribution of the injected signal. l_a represents the location of the start of the shield corrosion, which can be determined from the location results of $C_{sr}(t)$. Typically, l_c is considerably smaller than l_a and thus we approximate l_a as

$$l_a \approx \frac{t_p}{2} \cdot v_p, \tag{35}$$

$$v_p = \frac{2l_x}{t_x} \tag{36}$$

where v_p is the wave speed of the healthy cable, which can be measured from the healthy cable according to (36). t_x is the arrival time of the reflected signal from the open-circuit end.

In (32b), K_s is necessary for calculating l_c calculating. K_s is the characteristic parameter of the defects, and measuring K_s is extremely difficult, if not impossible. However, the model shown in Fig. 3 can be used to calculate it, leading to

$$K_s = \frac{d\beta_s}{d\omega}, \tag{37a}$$

$$\beta_s = \Im(\gamma_s), \tag{37b}$$

$$\gamma_s = \sqrt{(R_s + j\omega L_s)(G_s + j\omega C_s)}, \tag{37c}$$

where R_s, L_s, G_s, and C_s are the resistance, inductance, conductance, and capacitance of the shield corrosion defects, respectively.

In addition, the characteristic impedance Z_s of the shield corrosion defects can be calculated using double-frequency TFDR, yielding

$$Z_s = Z_p \frac{1+\Gamma_b}{1-\Gamma_b}, \tag{38a}$$

$$\Gamma_b = \frac{C_{r1}}{\sqrt{1 - \cos(K_s l_c \omega)^2}}. \tag{38b}$$

The complete steps of the double-frequency TFDR method for assessing the shield corrosion length are shown in Algorithm 1. To provide a clearer visualization of the double-frequency TFDR method for assessing the size of shield corrosion defects, a flowchart is presented in Fig. 6.

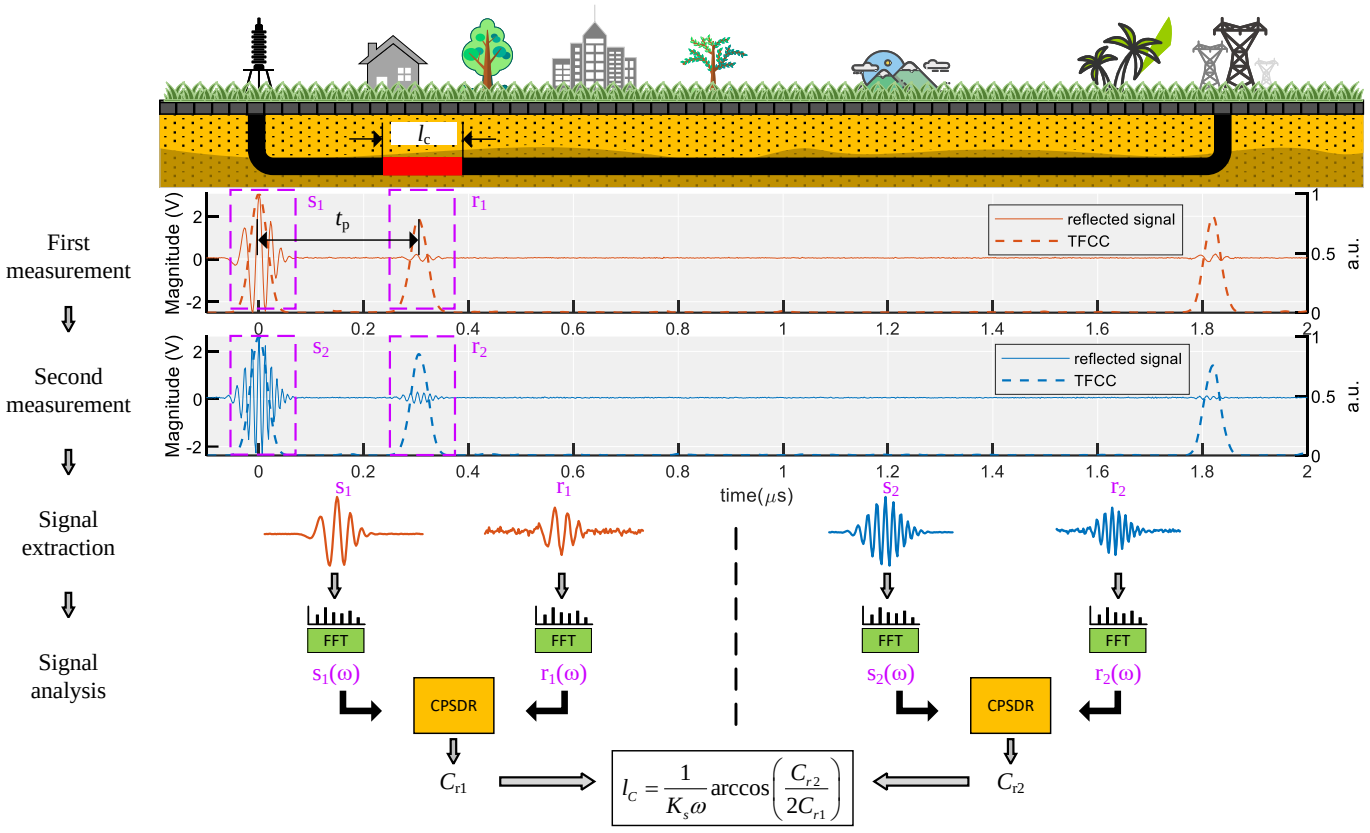

Fig. 6. Flowchart of the double-frequency TFDR.

Algorithm 1 Assessment of Shield Corrosion Length

1: Calculate α_p and v_p based on (34) and (36)
2: Model the shield corrosion defect and calculate K_s based on (16) and (37)
3: Initialize equipment and design injected signal $s_1(t)$
4: Perform the first measurement
5: Design injected signal $s_2(t)$ with double center frequency
6: Perform the second measurement
7: **for** each measurement result **do**
8: Calculate $C_{sr}(t)$ based on (3)
9: Perform defect location analysis
10: Extract the reflected signal $r(t + 2K_p l_a + K_s l_c)$
11: Calculate the spectra $S(\omega)$ and $R(\omega)$ using FFT
12: Calculate the spectrum ratio C_r based on (33)
13: **end for**
14: Perform the length evaluation based on (32b)
15: Output results and save data

To evaluate the performance of the double-frequency TFDR method, we analyze the algorithm complexity of its main steps and compare it with the traditional TFDR method. The complexity is presented in Table I. From Table I, we observe that our proposed method includes two additional steps with a complexity of $O(NlogN)$. However, the main complexity of both the proposed method and the traditional TFDR remains $O(MN^2)$.

TABLE I
ALGORITHM COMPLEXITY COMPERASION

main Steps	double-frequency TFDR	traditional TFDR
$W_s(t,\omega)$	$O(M^2)$	$O(M^2)$
$W_r(t,\omega)$	$O(N^2)$	$O(N^2)$
E_s	$O(M^2)$	$O(M^2)$
$E_r(t)$	$O(N^2)$	$O(N^2)$
$C_{sr}(t)$	$O(MN^2)$	$O(MN^2)$
$S(\omega)$	$O(MlogM)$	–
$R(\omega)$	$O(NlogN)$	–

III. Simulation and Results

This section simulates a 10-kV single-core cable to validate and demonstrate the double-frequency TFDR. First, we validate the shield corrosion model. Next, we demonstrate the use of double-frequency TFDR to assess the size of shield corrosion defects and confirm the effectiveness of the double-frequency TFDR approach.

A. Simulation of Shield Corrosion Defects

To verify the model for shield corrosion (15), a simulation was conducted using COMSOL Multiphysics 6.2, a FEM software. For the perfect cable, a 2D axisymmetric model of a 10 kV single-core cable was created directly, while for the cable with shield corrosion, a 3D model was built in SolidWorks, a 3D modeling software, and was imported into COMSOL for simulation. The specific parameters of the cable used in the simulation are detailed in Table II.

TABLE II
PARAMETERS OF THE 10-KV SINGLE-CORE CABLE.

Components	Size parameters (mm)	Electric parameters
Core	r = 3.335	γ_c = 5.98 $\times 10^7$ S/m
Inner-semiconductor	r = 4.115	$\epsilon = 500$
XLPE	r = 8.635	ϵ' = 2.3, ϵ'' = -0.001
Outer-semiconductor	r = 9.125	$\epsilon = 500$
Shield	r = 9.325, w = 31.3	γ_s = 5.98 $\times 10^7$ S/m
Sheath	r = 12.115	ϵ = 2.25

Note: r is the outer radius, w is the width of the copper shield tape.

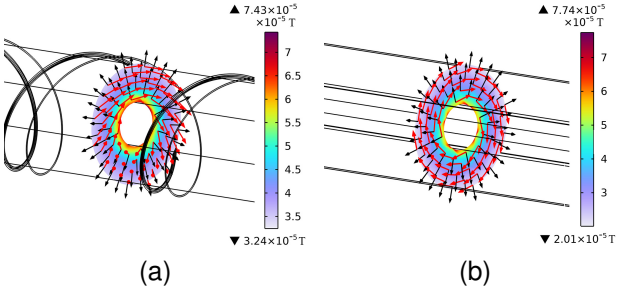

Fig. 7. Distribution of the magnetic flux density and electric field in the cable cross-section: (a) Cable with shield corrosion; (b) Healthy cable. The black arrows show the electric field direction and the red arrows show the magnetic field direction. The black lines are the outline of the cable structure. In (a), the black spiral lines represent shield tapes that have isolation between two adjacent layers caused by corrosion.

The electric and magnetic field distribution results are depicted in Fig. 7a. To illustrate the contrast with a healthy cable, the electric and magnetic field distribution for a healthy cable was also calculated using FEM and is presented in Fig. 7b.

In Figure 7a, the magnetic flux is characterized not only by its circumferential magnetic field but also by an axial component. Focusing on a cable with a 15% shield overlap, the inductance L_{sc} attributed to a shield corrosion defect is calculated using FEM to be 356.8 nH/m. In contrast, the result derived from the shield corrosion model (SCM), as specified in (15), is 364.4 nH/m. Additionally, we have conducted a comparative analysis of both simulation and calculation results for shields exhibiting corrosion at various overlap ratios. This comparison is detailed in Table III.

TABLE III
COMPARION OF L_{sc} VALUES CALCULATED BY FEM AND SCM.

Samples	ρ	L_{FEM}(nH/m)	L_{SCM}(nH/m)	error
Cable I[1]	5%	266.6	271.8	-2.0%
	10%	307.9	314.2	-2.1%
	15%	356.8	364.4	-2.1%
Cable II[2]	5%	228.0	232.2	-1.8%
	10%	265.0	270.1	-1.9%
	15%	308.6	314.9	-2.0%

[1] The radius of the cable shield is 9.325mm.
[2] The radius of the cable shield is 8.625mm.

In Table III, the results obtained from FEM and the SCM compare very well, with the maximum discrepancy being 2.1%. This indicates that the SCM is an effective model for expressing the inductance associated with shield corrosion defects.

B. Simulation of Long Cables with Shield Corrosion Defects

In this section, we simulated a TFDR signal propagating over a long cable with shield corrosion defects and analyzed the effect of these defects on the reflected signals. According to (21), the transfer function $H_c(\omega)$ of a long cable with shield corrosion defects is essential for calculating the reflected signal $r(t)$. The transfer function $H_c(\omega)$ corresponds to the S_{11} parameter in $\boldsymbol{S}_c$, the scattering matrix of a long cable with defects. The $\boldsymbol{S}_c$ of a long cable with defects can be viewed as a cascade model consisting of two long healthy cables and a cable section with a defect. When cascading the defective and healthy cables, the $\boldsymbol{S}$ matrix needs to be converted into the transmission matrix $\boldsymbol{T}$ [34]. The cascading action is more straightforwardly expressed using the $\boldsymbol{T}$ matrix. The overall transmission matrix $\boldsymbol{T}_c$ of a long cable with cable shield corrosion defects is found as

$$\boldsymbol{T}_c = \boldsymbol{T}_{p1} \cdot \boldsymbol{T}_s \cdot \boldsymbol{T}_{p2} \cdot \boldsymbol{T}_o, \tag{39}$$

where $\boldsymbol{T}_{p1}$, $\boldsymbol{T}_s$, and $\boldsymbol{T}_{p2}$ represent the transmission matrices of the first healthy cable section, the defective section, and the second healthy section, respectively, whereas $\boldsymbol{T}_o$ denotes the transmission matrix of a high-impedance component that simulates an open terminal.

The reflected signal $r(t)$ of a long cable with defects is calculated as

$$r(t) = \mathcal{F}^{-1}\left(S(\omega) \cdot S_{c,11}\right), \tag{40}$$

where $S_{c,11}$ is the S_{11} parameter in $\boldsymbol{S}_c$.

In the context of (40), besides $H_c(\omega)$, the injected signal $s(t)$ is essential for calculating $r(t)$. The parameters of $s(t)$ are mainly determined by the cable attenuation constant, cable length, noise level on-site, and the performance of the signal equipment. Referring to the design method of $s(t)$ in [25], [35], to achieve a maximum measurable length of a 1000-meter-long 10 kV cable, we set the fundamental frequency signal s_1 to have $\omega_0 = 40$ MHz, a bandwidth of 40 MHz, and with $t_0 = 100$ ns.The double-frequency signal $s_2(t)$ has $\omega_0 = 80$ MHz, a bandwidth of 40 MHz, and with $t_0 = 100$ ns. These two signals are sequentially injected into a 250-meter cable for two continuous cable measurements. Taking the measurement results of $s_1(t)$ as an example, the reflected signal $r(t)$ is shown in Fig. 8 for various shield corrosion defects.

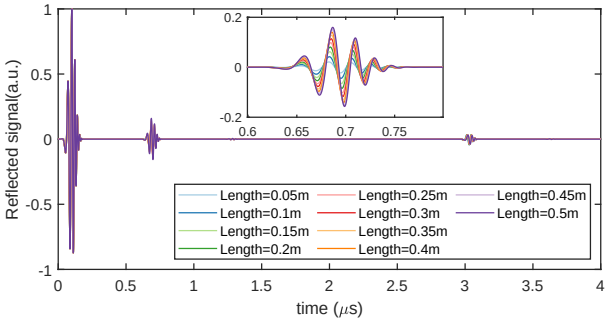

Fig. 8. Reflected signals for various shield corrosion types and sizes.

In Fig. 8, the signals observed near 0 μs represent the injected signal. The reflected signals appearing at around

0.7 μs are caused by the reflections from the defects, while signals located near 3 μs result from reflections at the open terminal of the cable. By comparing the reflected signals, we observe that the magnitude of the reflected signals increases as the defect length increases, and the arrival time of the reflected signals is delayed with increasing defect length. This is consistent with the results in reference [24].

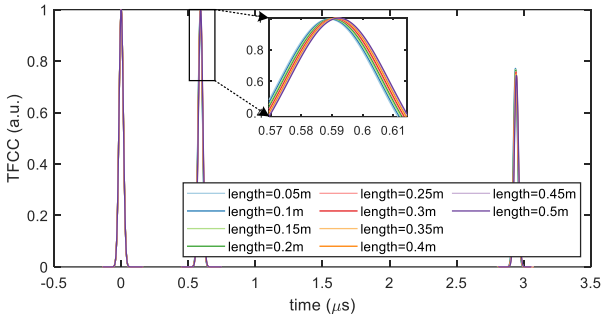

Fig. 9. Effect of various shield corrosion sizes on the location of the peak in TFCC curves.

The defects depicted in Fig. 8 are located using the TFCC method, and the corresponding location curves are presented in Fig. 9. In Fig. 9, the time corresponding to the location of defects is marked by the occurrence of the second peaks. The peaks around 1.2 μs represent the second reflection of the injected signal at the defect location, while peaks near 3 μs refer to the reflections from the cable end. In Fig. 9, the timing of the second peaks is observed to be delayed as the defect length increases. This conclusion is consistent with the results of (27).

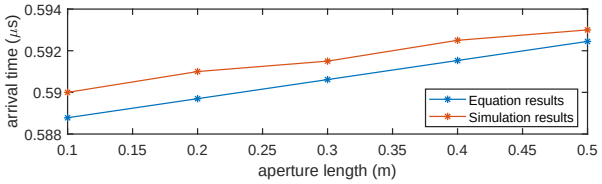

Fig. 10. Effect of the defect length on the location: comparison between simulations and equations.

The comparison on the arrival time of the reflected signal obtained from the simulations and with the analytical model is shown in Fig. 10. In Figs. 10, we find some differences between the simulation and the equation results. This is caused by the simulation time step and by the approximations in (19) and (20).

To assess the size of shield corrosion defects, the characteristic parameter K_s must be calculated using equations (5), (7), (8), (16), and (37). For the cable specified in Table II, the value of K_s is 9.1656×10^{-9} s/m. The value of α_p is 0.0066 m^{-1} at a center frequency of 40 MHz and 0.0119 m^{-1} at 80 MHz. The evaluation results of corrosion size using double-frequency TFDR are shown in Fig. 11 for defects ranging from 0.05 m to 0.5 m in length.

From Fig. 11, we can see that there are some differences between the evaluated values and the reference. These are mainly

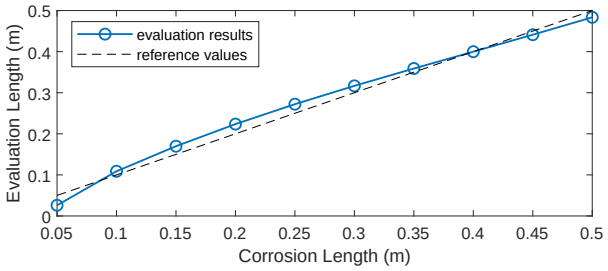

Fig. 11. Assessment results of shield corrosion size using the double-frequency TFDR

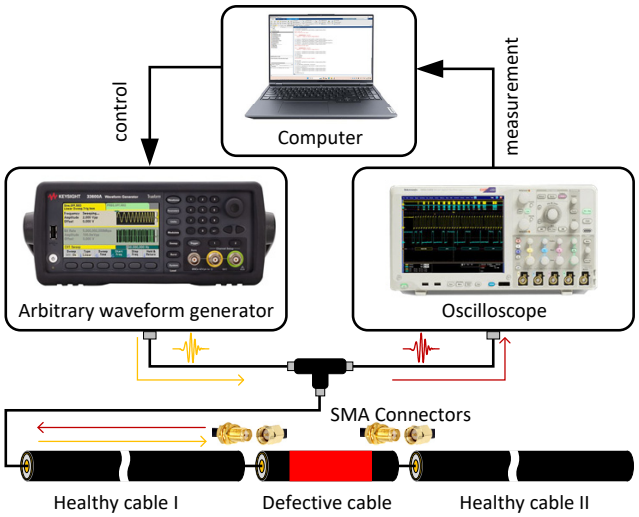

Fig. 12. Schematic of the experiment.

caused by the approximation of the reflection coefficient of the defect, as shown in (20).

IV. Experiments and Results

To validate the proposed shield corrosion models and evaluate the effectiveness of the proposed method in assessing the size of cable shield corrosion defects, an experiment was conducted. The schematic of the experimental setup is depicted in Fig. 12.

The experiment platform consists of an arbitrary waveform generator that generates the injected signal for the TFDR, an oscilloscope that captures the reflected signals, a computer that processes and analyzes the reflected signals, and two long cables serving as healthy sections of the measured cable. Additionally, short cable sections with different defects are designed to be inserted between the two healthy sections. In the experiment, the cable was a SYV50 cable. There are two reasons for this choice: first, the SYV50 cable has a similar coaxial structure as the power cable. Second, the SMA connector has a 50 Ω characteristic impedance and matches the SYV50 cable perfectly [36]. The short defective cables are inserted between two long healthy cables using SMA connectors, which reduces the effect of such a connection on the reflected signals of the defects. The experiment setup is shown in Fig. 13. In the experiment, the arbitrary waveform

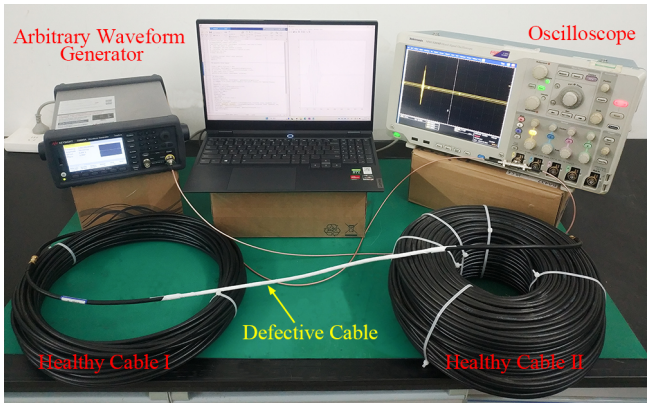

Fig. 13. Experiment setup.

generator used is the Keysight 33621A, and the oscilloscope is the Tektronix MSO5204B. The data is analyzed using data analysis programs that we coded according to the above equations in MATLAB 2022a.

Defective cable sections were exemplified in Fig. 2. To mimic the isolation caused by corrosion between the shield tapes of adjacent layers, a thin Scotch tape is inserted between them. Two cable samples are fabricated with lengths of 20 cm and 30 cm.

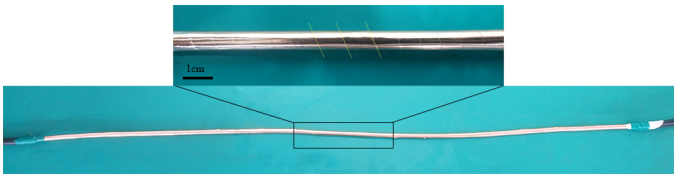

Fig. 14. Cable samples mimicking shield corrosion defects.

Fig. 15 shows the measurement results for two cable samples with corrosion defects. To validate the model of Fig. 4, we simulated the experiment, and the corresponding results are shown in Fig. 16.

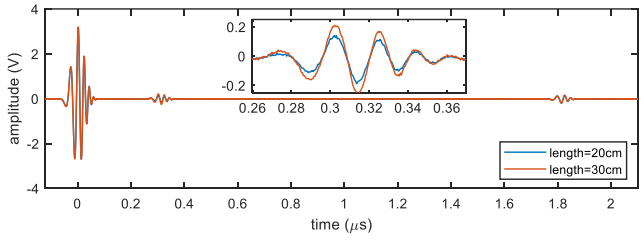

Fig. 15. Effect on reflected signals of the defect length for a shield corrosion.

Defects are located using the TFCC method. The TFCC curves of the reflected signals are plotted in Fig. 17. The peaks occur at the start and end points of the cable, as well as at locations where defects are present. Therefore, defects can be identified by determining the time corresponding to these peak occurrences. In Fig. 17, the time corresponding to defects is 0.295 μs.

To determine the location of the defects and calculate the defect length, the phase velocity and attenuation α_p of the

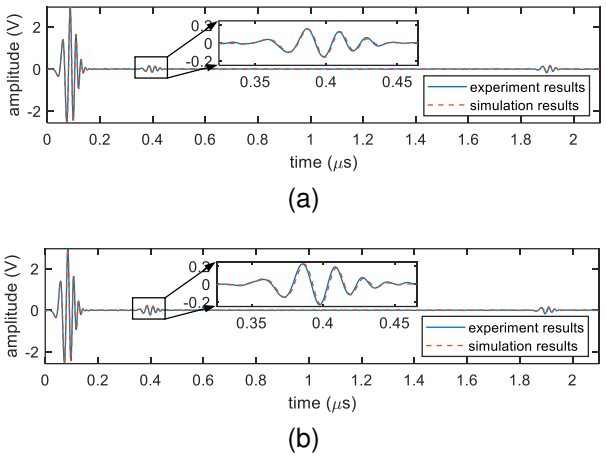

Fig. 16. Comparison between the reflected signals obtained with the experiment and in simulation for shield corrosion defects with a length of 20 cm (a) and 30 cm (b).

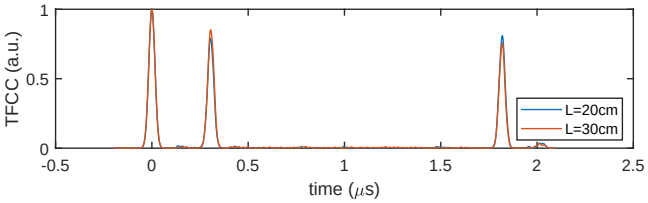

Fig. 17. TFCC curves showing the location of the defects in the cable.

SYV50 cable were measured according to (36) and (34), and K_s was calculated according to (37). The measured v_p is 204.08 m/μs, and the attenuation α_p is 0.0072 m^{-1} at 40 MHz and 0.0085 m^{-1} at 80 MHz, whereas the K_s is 7.1695e-09 s/m.

TABLE IV
COMPARISON BETWEEN ACTUAL DEFECT SIZES AND THEIR ESTIMATES USING DOUBLE-FREQUENCY SIGNALS.

defect size	L_e[1](cm)	error
20 cm	20.006	0.3%
30 cm	30.001	0.03%

[1] L_e is the estimated value of the defect length.

According to (32), the lengths of defects in the experiment are estimated and the results are shown in Table IV. From the comparison in Table IV, we can conclude that the double-frequency TFDR is a valid method for evaluating the size of cable shield corrosion defects. The estimations are very accurate, and the error between observed and estimated values is less than 1%. This difference in error magnitude can be attributed not only to the approximation of the reflection coefficient, as described in (20), but also to the influence of noise on the measurement process, which will be addressed in future works.

Also, we calculated the characteristic impedance Z_s of shield corrosion defects using (38) and compared the measured Z_s with the values obtained from the shield corrosion models, as shown in Fig. 3. The simulated and measured results of Z_s are presented in Table V. The error between measured

TABLE V
COMPARISON BETWEEN SIMULATED AND MEASURED VALUES OF Z_s.

defect size	simulated Z_s	measured Z_s	error
20 cm	72.84	74.58	2.40%
30 cm	72.84	72.21	-0.87%

and simulated values is less than 2.4%, which proves that the double-frequency TFDR can accurately measure the characteristic impedance of cable shield corrosion defects. In addition, the results in Table V reveal that, for shield corrosion, the value of Z_s is almost constant and further validate the models of shield corrosion defects.

V. CONCLUSION

This article proposed a method leveraging double-frequency TFDR for detecting and evaluating cable shield corrosion defects, refining the measurement approach of conventional TFDR. While traditional TFDR precisely locates shield corrosion defects, it falls short in assessing defect sizes. Building upon TFDR, the double-frequency TFDR methodology incorporates a shield corrosion model, a secondary measurement technique, and an analysis method based on the spectrum ratio, enabling precise evaluation of shield corrosion length.

The double-frequency TFDR was confirmed as an effective method for locating and assessing the size of shield corrosion defects. Compared to the existing TFDR method, the double-frequency TFDR method provides additional information about defect size, which can help the crew evaluate the severity of the defects and develop a maintenance plan. Additionally, the proposed method can enhance both the development of digital twin technology and condition awareness technology for power cables.

The greatest advantage of this method is that it can evaluate the defect length solely by improving the measurement strategy and signal analysis method, without the need for additional equipment, compared to the conventional TFDR method. However, in the experiment, we observed that the errors in the results were mainly caused by noise. Therefore, future work will focus on analyzing the influence of noise and developing appropriate noise reduction techniques.

REFERENCES

[1] G. Zhu, Z. Liu, K. Zhou, Z. Wang, L. Lu, Y. Li, and P. Meng, "A novel dampness diagnosis method for distribution power cables based on time-frequency domain conversion," *IEEE Trans. Instrum. Meas.*, vol. 71, pp. 1–9, 2022.

[2] L. Bai, M. Su, L. Sun, S. Fan, S. Xun, M. Huang, and H. Peng, "Mechanism characterization and nondestructive inspection method of thermal degradation faults in epdm cable termination," *IEEE Trans. Instrum. Meas.*, vol. 71, pp. 1–12, 2022.

[3] Y. Sebbane, A. Boubakeur, and A. Mekhaledi, "Influence of thermal aging and water adsorption on xlpe cables insulation mechanical and physico-chemical properties," *IEEE Trans. Dielectr. Electr. Insul.*, vol. 28, no. 5, pp. 1694–1702, 2021.

[4] Y. Zhou, Y. Zhang, L. Zhang, D. Guo, X. Zhang, and M. Wang, "Electrical tree initiation of silicone rubber after thermal aging," *IEEE Trans. Dielectr. Electr. Insul.*, vol. 23, no. 2, pp. 748–756, 2016.

[5] Y. Chen, B. Hui, Y. Cheng, Y. Hao, M. Fu, L. Yang, S. Hou, and L. Li, "Failure investigation of buffer layers in high-voltage XLPE cables," *Eng. Failure Anal.*, vol. 113, p. 104546, 2020.

[6] "IEEE guide for assessment, mitigation, and control of corrosion of metallic shields for extruded dielectric cables rated 5 kv to 46 kv," *IEEE Std 1617-2022*, pp. 1–40, 2023.

[7] U. Patel, "The impact of harmonics on the power cable stress grading system," Master's thesis, University of Waterloo, 2012.

[8] "IEEE guide for detection, mitigation, and control of concentric neutral corrosion in medium-voltage underground cables," *IEEE Std 1617-2007*, pp. C1–18, 2007.

[9] C. K. Lee, K. Seok Kwak, J. B. Park, and T. S. Yoon, "Concentric neutrals corrosion localization and its impedance analysis in the underground power cable system based on the reflectometry," in *2012 IEEE International Instrumentation and Measurement Technology Conference Proceedings*, 2012, pp. 1148–1153.

[10] R. J. Hamidi, S. H. Hosseinian, S. H. H. Sadeghi, and Z. Qu, "A novel approach to utilize plc to detect corroded and eroded segments of power transmission lines," *IEEE Trans. Power Del.*, vol. 30, no. 2, pp. 746–754, 2015.

[11] R. J. Totten, "Unintentional rf radiation and reception in coaxial cable transmission lines due to sheath conductor faults," Ph.D. dissertation, University of New Hampshire, 2018.

[12] I. Muchaidze, "Installation and performance evaluation of coaxial cable sensors for crack and corrosion detection," Ph.D. dissertation, Missouri University of Science and Technology, 2011.

[13] G. D. Chen, S. S. Sun, D. Pommerenke, J. L. Drewniak, G. G. Greene, R. D. McDaniel, A. Belarbi, and H. M. Mu, "Crack detection of a full-scale reinforced concrete girder with a distributed cable sensor," *Smart Mater. Struct.*, vol. 14, no. 3, p. S88, may 2005.

[14] D. Ju, G. Chu, Y. Liang, J. Huang, and W. Bai, "Fault identification and localization for cables based on time-frequency domain reflection," in *2023 IEEE International Conference on Control, Electronics and Computer Technology (ICCECT)*, 2023, pp. 896–900.

[15] J. J. Guo and S. A. Boggs, "High frequency signal propagation in solid dielectric tape shielded power cables," *IEEE Trans. Power Del.*, vol. 26, no. 3, pp. 1793–1802, 2011.

[16] F. Auzanneau, "Multiple soft defect signature magnification in electrical cables with binary time-domain reflectometry," *IEEE Sens. Lett.*, vol. 4, no. 7, pp. 1–4, 2020.

[17] H.-B. Mu, H.-T. Zhang, X.-Y. Zou, D.-N. Zhang, X. Lu, and G.-J. Zhang, "Sensitivity improvement in cable faults location by using broadband impedance spectroscopy with dolph-chebyshev window," *IEEE Trans. Power Del.*, vol. 37, no. 5, pp. 3846–3854, 2022.

[18] X.-Y. Zou, H.-B. Mu, H.-T. Zhang, L.-Q. Qu, Y.-F. He, and G.-J. Zhang, "An efficient cross-terms suppression method in time-frequency domain reflectometry for cable defect localization," *IEEE Trans. Med. Imag.*, vol. 71, pp. 1–10, 2022.

[19] E. Song, Y.-J. Shin, P. E. Stone, J. Wang, T.-S. Choe, J.-G. Yook, and J. B. Park, "Detection and location of multiple wiring faults via time-frequency-domain reflectometry," *IEEE Trans. Electromagn. Compat.*, vol. 51, no. 1, pp. 131–138, 2009.

[20] H. Lim, G.-Y. Kwon, and Y.-J. Shin, "Fault detection and localization of shielded cable via optimal detection of time-frequency-domain reflectometry," *IEEE Trans. Instrum. Meas.*, vol. 70, pp. 1–10, 2021.

[21] X. Zou, H. Mu, R. Wang, K. Fan, Z. Cheng, Y. He, and G. Zhang, "An efficient accuracy improvement method for cable defect location based on instantaneous filtering in time-frequency domain," *Measurement*, vol. 226, p. 114178, 2024.

[22] H. Lim, Y. H. Lee, S. S. Bang, and Y.-J. Shin, "Application of enhanced optimal-detection of time–frequency domain reflectometry on hts cable with high-resolution," *IEEE Trans. Appl. Supercond.*, vol. 33, no. 5, pp. 1–10, 2023.

[23] G.-Y. Kwon, C.-K. Lee, and Y.-J. Shin, "Diagnosis of shielded cable faults via regression-based reflectometry," *IEEE Trans. Ind. Electron.*, vol. 66, no. 3, pp. 2122–2131, 2019.

[24] A. Manet, A. Kameni, F. Loete, J. Genoulaz, L. Pichon, and O. Picon, "Equivalent circuit model of soft shield defects in coaxial cables using numerical modeling," *IEEE Trans. Electromagn. Compat.*, vol. 59, no. 2, pp. 533–536, 2017.

[25] Y.-J. Shin, E. Powers, T.-S. Choe, C.-Y. Hong, E.-S. Song, J.-G. Yook, and J. B. Park, "Application of time-frequency domain reflectometry for detection and localization of a fault on a coaxial cable," *IEEE Trans. Instrum. Meas.*, vol. 54, no. 6, pp. 2493–2500, 2005.

[26] S. J. Chang and G.-Y. Kwon, "Anomaly detection for shielded cable including cable joint using a deep learning approach," *IEEE Trans. Instrum. Meas.*, vol. 72, pp. 1–10, 2023.

[27] B. Boashash, *Time-frequency signal analysis and processing: a comprehensive reference*. Academic press, 2015.

[28] C. R. Paul, *Analysis of Multiconductor Transmission Lines*, 2nd ed. Wiley-IEEE Press, 2007.
[29] P. C. J. M. v. d. Wielen, "On-line detection and location of partial discharges in medium-voltage power cables," Ph.D. dissertation, Eindhoven University of Technology, 2005.
[30] M. Tozzi, A. Cavallini, G. C. Montanari, and G. G. Burbui, "PD detection in extruded power cables: an approximate propagation model," *IEEE Trans. Dielectr. Electr. Insul.*, vol. 15, no. 3, pp. 832–840, 2008.
[31] T. Ohtsuka and T. Komatsu, "Enhancement of electric conductivity of the rust layer by adsorption of water," *Corros. Sci.*, vol. 47, no. 10, pp. 2571–2577, 2005.
[32] C. R. Paul, *Inductance: loop and partial*. John Wiley & Sons, 2011.
[33] X.-D. Zhang, *Modern signal processing*. Walter de Gruyter GmbH & Co KG, 2022.
[34] D. M. Pozar, *Microwave engineering*. John wiley & sons, 2011.
[35] J. Wang, P. Stone, Y.-J. Shin, and R. Dougal, "Application of joint time-frequency domain reflectometry for electric power cable diagnostics," *IET Signal Process.*, vol. 4, no. 4, pp. 395–405, 2010.
[36] J. P. Dunsmore, *Handbook of microwave component measurements: with advanced VNA techniques*. John Wiley & Sons, 2020.

Kun Zhao (Student Member, IEEE) received the B.S. degree in electrical engineering from the Chinese University of Mining and Technology, Xuzhou, China, in 2017 and the M.S. degree in high voltage and insulation technology from HoHai University, Nanjing China, in 2020.

He is currently working towards a Ph.D. in electrical engineering at Xi'an Jiaotong University and with the Department of Electronics and Telecommunications, Politecnico di Torino, Turin, Italy. His main research interests include diagnosing electrical equipment, modeling electromagnetic, and signal processing.

Stefano Grivet-Talocia (Fellow, IEEE) received the Laurea and Ph.D. degrees in electronic engineering from the Politecnico di Torino, Turin, Italy, in 1994 and 1998, respectively.

From 1994 to 1996, he was with the NASA/Goddard Space Flight Center, Greenbelt, MD, USA. He is currently a Full Professor of electrical engineering with the Politecnico di Torino. He co-founded the academic spinoff company IdemWorks, Turin, in 2007, serving as the President until its acquisition by CST in 2016. He has authored about 200 journal and conference papers. His current research interests include passive macromodeling of lumped and distributed interconnect structures, model-order reduction, modeling and simulation of fields, circuits, and their interaction, wavelets, time-frequency transforms, and their applications.

Dr. Grivet-Talocia was a co-recipient of the 2007 Best Paper Award from the IEEE TRANSACTIONS ON ADVANCED PACKAGING. He received the IBM Shared University Research Award in 2007, 2008, and 2009. He was the General Chair of the 20th and 21st IEEE Workshops on Signal and Power Integrity (SPI2016 and SPI2017). He was an Associate Editor of the IEEE TRANSACTIONS ON ELECTROMAGNETIC COMPATIBILITY from 1999 to 2001 and he is currently serving as an Associate Editor for the IEEE TRANSACTIONS ON COMPONENTS, PACKAGING AND MANUFACTURING TECHNOLOGY.

Paolo Manfredi (Senior Member, IEEE) received the M.Sc. degree in electronic engineering and the Ph.D. degree in information and communication technology from the Politecnico di Torino, Turin, Italy, in 2009 and 2013, respectively.

From 2014 to 2017, he was a Post-Doctoral Research Fellow of the Research Foundation-Flanders (FWO) with the Electromagnetics Group, Department of Information Technology, Ghent University, Ghent, Belgium. He is currently an Associate Professor with the EMC Group, Department of Electronics and Telecommunications, Politecnico di Torino. His research interests comprise the several aspects of circuit and interconnect modeling and simulation, including uncertainty quantification, surrogate modeling, signal integrity, and electromagnetic compatibility.

Dr. Manfredi was a recipient of the Outstanding Young Scientist Award at the 2018 Joint IEEE International Symposium on Electromagnetic Compatibility and Asia-Pacific Symposium on Electromagnetic Compatibility, the Best Paper Award at the 2016 IEEE Electrical Design of Advanced Packaging and Systems Symposium, the Best Oral Paper Award and the Best Student Paper Award at the 22nd, and 19th IEEE Conference on Electrical Performance of Electronic Packaging and Systems, respectively, a Young Scientist Award at the XXX International Union of Radio Science General Assembly and Scientific Symposium, and an Honorable Mention at the 2011 IEEE Microwave Theory and Techniques Society International Microwave Symposium. He is currently serving as an Associate Editor for the IEEE JOURNAL ON MULTISCALE AND MULTIPHYSICS COMPUTATIONAL TECHNIQUES and the International Journal of Circuit Theory and Applications, and as an Academic Editor for Mathematical Problems in Engineering.

Yuan Yan was born in Sichuan, China, in 1996. He received the B.S. degree in electrical engineering from Xi'an Jiaotong University, Xi'an, China, in 2018.

He is currently working toward the Ph.D. degree in electrical engineering at Xi'an Jiaotong University, and also with the Department of Electronics and Telecommunications, Politecnico di Torino, Turin, Italy. His research interests mainly include the insulation condition monitoring of electrical equipment, modeling of electromagnetic, and signal processing.

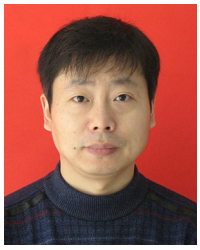

Hongjie Li was born in Henan, China, in 1966. He received the B.S., M.S., and the Ph.D. degrees from Xi'an Jiaotong University, Xi'an, China, in 1989, 1992, and 1998, respectively. In 1997, he was a Visiting Scholar with Osaka University, Osaka, Japan. From 1999 to 2001, he was a Research Fellow on insulation condition monitoring with Nanyang Technological University, Singapore.

From 2001 to 2007, he was employed with Singapore Power Grid Company, Ltd. He is currently a Professor with the High Voltage Division, School of Electrical Engineering, Xi'an Jiaotong University. His main research interests include insulation condition monitoring of electrical equipment, modeling, and numerical analysis of electromagnetic.